

# Determination of the Sunshape from Meteosat Second Generation

SFERA Project Report  
Work Package 13 - Task 1 (E)  
Deliverable R13.4

Bernhard Reinhardt\*, Robert Buras<sup>†</sup>, Luca Bugliaro\*, Bernhard Mayer<sup>†</sup>

July 14, 2012

Version 1.7

---

\*Deutsches Zentrum für Luft- und Raumfahrt e.V., Institut für Physik der Atmosphäre,  
Oberpfaffenhofen, Wessling, Germany

<sup>†</sup>Meteorologisches Institut München, Ludwig-Maximilians-Universität, München, Germany

# Contents

<b>Glossary</b>	<b>2</b>
<b>1 Introduction</b>	<b>3</b>
<b>2 Definitions</b>	<b>4</b>
2.1 Sunshape and Circum Solar Ratio . . . . .	4
2.2 Effective Radius . . . . .	4
2.3 Ice Particle Shapes . . . . .	5
<b>3 Ice Cloud Property Retrieval from MSG</b>	<b>5</b>
3.1 Description of APICS . . . . .	5
3.2 Cloud Detection . . . . .	6
3.3 Retrieval of Optical and Microphysical Properties . . . . .	6
3.4 Improvements Obtained Using a New Albedo Source . . . . .	7
<b>4 Improvements in Radiative Transfer Modelling</b>	<b>11</b>
<b>5 Parametrization of Circum Solar Radiation</b>	<b>12</b>
5.1 Sensitivity to Neglected Parameters . . . . .	13
5.1.1 Rayleigh Scattering . . . . .	13
5.1.2 Albedo . . . . .	14
5.2 Concept of the Apparent Optical Thickness . . . . .	14
5.3 Uncertainty due to Unknown Ice Particle Shape . . . . .	16
<b>6 Circum Solar Radiation Retrieval from MSG</b>	<b>19</b>
6.1 Circum Solar Ratios for Different Ice Particle Shapes . . . . .	19
6.2 Influence of the Cloud Mask on Retrieved Circum Solar Ratios . . . . .	23
6.3 Circum Solar Irradiance . . . . .	26
<b>7 Conclusion</b>	<b>28</b>

## Glossary

$I$	Normal irradiance
$L$	Radiance
$\alpha$	Angular distance from the center of the sun
$\phi$	Relative azimuth
$\tau$	Optical thickness in vertical direction
$\tau_a$	Apparent optical thickness (slant path) of particulate matter (molecular extinction excluded)
$\tau_s$	Slant path optical thickness of particulate matter (molecular extinction excluded)
$\theta_{\text{sat}}$	Satellite zenith angle
$\theta_{\text{sun}}$	Sun zenith angle
$r_{\text{eff}}$	Effective radius
APICS	Algorithm for the Physical Investigation of Clouds
BRDF	Bidirectional Reflectance Distribution Function
COCS	Cloud Optical properties derived from CALIOP and SEVIRI algorithm
CSP	Concentrating Solar Power
CSR	Circum Solar Ratio
FOV	Circular Field of View (Given as opening half angle)
LUT	Lookup Table
MISR	Multi-Angle Imaging SpectroRadiometer (aboard NASA's polar orbiting satellite Terra)
MODIS	Moderate-Resolution Imaging Spectroradiometer (aboard NASA's polar orbiting satellites Terra and Aqua)
MSG	Meteosat Second Generation meteorological satellite series
SAM	Sun and Aureole Measurement System
SEVIRI	Spinning Enhanced Visible Infra-Red Imager (aboard the MSG satellites)

# 1 Introduction

The Work Package (WP) 13 aims at establishing knowledge on how to achieve ultra-high flux concentration in concentrating solar power (CSP) facilities – especially by the use of secondary concentrators. For the design and the precise evaluation of high flux concentrators the radiance distribution inside and around the sun disk, called sunshape, should be known.

Due to a strong angular radiance gradient – spanning several orders of magnitude – the sunshape is difficult to measure (Wilbert et al. 2011). Task 1-A and 1-B of WP 13 aim at the development of a device to measure the sunshape directly on the ground that can be replicated and deployed at different sites. In sub-task 1-E which is covered by this report a method was developed to provide information about the sunshape on a global scale utilizing geostationary satellites. In this project measurements of the Spinning Enhanced Visible Infra-Red Imager (SEVIRI) aboard the geostationary meteorological satellites of the Meteosat Second Generation (MSG) series were used.

Circum solar radiation is caused by scattering of the sun light by atmospheric particles. Considering a homogeneous atmosphere the radiance decreases with angular distance from the sun. The steepness and shape of this angular gradient depends on the particle’s type, shape and size as well as on the optical thickness.

Three relevant particle types can be distinguished: Droplets of water clouds, ice crystals of cirrus clouds and aerosol particles. Water clouds are usually optically thick and extinguish too much light to allow for CSP operation. In contrast, aerosols are optically much thinner so that the possibilities to characterize them with SEVIRI are only very limited, especially over arid regions that are of special interest for CSP operation. Due to this limitations the focus of this study lies on cirrus clouds. These ice clouds often occur within an optical thickness range that on one hand still allows the operation of CSPs and on the other hand makes them detectable with satellites.

Note that some developments described in this report are also applicable to aerosols (Secs. 4 and 5). Work is ongoing beyond this project to evaluate the usability of the ECMWF’s Integrated Forecast System (IFS) as aerosol input to circum solar radiation modeling on global scale. The results of this evaluation are expected to be part of a dissertation in spring 2013 (Reinhardt 2013).

Our method to derive the circum solar radiation comprises of two steps. First the particle size and optical depth of the cirrus clouds are determined using the Algorithm for the Physical Investigation of Clouds with SEVIRI (APICS) (Bugliaro et al. 2011; Bugliaro et al. 2012). A parametrization is then applied to convert these parameters into circum solar radiation. This parametrization was developed during the project based using simulations of the sunshape with the radiative transfer model MYSTIC (Mayer 2009).

The remainder of the document is structured as follows. In Sec. 2 basic definitions are made. The difficulties of detecting and retrieving properties of thin cirrus clouds with APICS and achieved improvements in this field are outlined in Sec. 3. The problems and found solutions considering the exact simulation

of the sunshape with MYSTIC that is necessary for the development of our parametrization of the circum solar radiation is described in Sec. 4 . This parametrization that converts cloud properties to circum solar radiation is developed in Sec. 5. In Sec. 6 we apply the method to SEVIRI data. We also discuss the impact of two different cloud detection schemes (see Sec. 3.2) as well as of the ice particle shape that so far cannot be determined from MSG. A conclusion is given in Sec. 7.

## 2 Definitions

### 2.1 Sunshape and Circum Solar Ratio

The one-dimensional radiance distribution along a radial cut from the sun center to the outside is called sunshape. The circum solar ratio (CSR) is a common scalar quantity that can be used to characterize the sunshape (Buie et al. 2003). The CSR is defined as the normal irradiance coming from the circum solar region divided by the normal irradiance from the sun disk and the circum solar region. For the remainder of the document the term irradiance always refers to irradiance on a surface perpendicular to the direction pointing at the sun. The circum solar region is described by the angle  $\alpha_{\text{cir}}$  which is its limiting angular distance to the center of the sun disk. With this we can write

$$\text{CSR} = \frac{\int_0^{2\pi} \int_{\alpha_{\text{sun}}}^{\alpha_{\text{cir}}} L(\alpha) \sin(\alpha) d\alpha d\phi}{\int_0^{2\pi} \int_0^{\alpha_{\text{cir}}} L(\alpha) \sin(\alpha) d\alpha d\phi}. \quad (1)$$

where  $L$  denotes the radiance depending on the angular distance  $\alpha$  from the sun center. The disk angle  $\alpha_{\text{sun}}$  is measured from the sun center to its edge.

Instead of deriving the sunshape we focus on the ability to derive the CSR for arbitrary limiting angles. However, the sunshape can be reproduced by applying our parametrization multiple times for different angles (see Sec. 5).

### 2.2 Effective Radius

In the atmosphere particles are not monodisperse but appear in different size distributions. To quantify a single size measure that is optically relevant we use the effective radius  $r_{\text{eff}}$ . The effective radius is defined by

$$V = \int V(D)n(D)dD, \quad (2)$$

$$A = \int A(D)n(D)dD, \text{ and} \quad (3)$$

$$r_{\text{eff}} = \frac{3V}{4A}. \quad (4)$$

Where  $n$  is the size distribution,  $A$  the projected area and  $V$  the volume of the particles. By  $D$  we denote the maximum dimension of the particles but in general it could be any particle scale (q.v. Baum et al. (2005a) and Schumann et al. (2010)).

### 2.3 Ice Particle Shapes

Passive remote sensing methods like APICS cannot retrieve information concerning ice particle shapes. To assess the uncertainty that is caused by not knowing the ice particle shape we use a range of cloud bulk optical properties for the simulation of the circum solar radiation as well as for the cloud property retrieval. Clouds consisting solely of particles of a single shape as well as shape mixtures are considered.

The particle mixtures and associated optical properties are described in Baum et al. (2005a), Baum et al. (2005b) and Baum et al. (2011). We call the older version “baum\_v2” and the newer version “baum\_v3.5”. The later incorporates more particle shapes and the particle surface is “severely roughened” while “baum\_v2” is composed of particles with flat surfaces. The five different single particle shapes that are considered comprise solid-columns, hollow-columns, rough-aggregates, rosettes, and droxtals. The bulk optical properties for these have been generated by Claudia Emde (Pers. Comm.) using single scattering properties by Hong Gang which in turn are based on models by Yang et al. (2000). All optical property datasets expose an effective radius range of  $5\mu m - 90\mu m$ , except for “baum\_v3.5” which covers  $5\mu m - 60\mu m$ . Not all combinations of a single particle shape and effective radius are expected to exist in reality – for example Baum et al. (2005a) used aggregates only as representation of very large particles. Nevertheless, the considered optical properties are expected to cover a large part of the natural variability.

## 3 Ice Cloud Property Retrieval from MSG

### 3.1 Description of APICS

This study relies on the Algorithm for the Physical Investigation of Clouds with SEVIRI (APICS) framework (Bugliaro et al. 2011; Bugliaro et al. 2012) to derive effective radius and optical thickness of the cirrus clouds. APICS implements a cloud property retrieval based on Nakajima and King (1990) for the SEVIRI channels 1 and 3 in the solar spectrum (centered at  $0.6\mu m$  and  $1.6\mu m$ ). Currently it is assumed that the channels 1 and 3 of the SEVIRI instrument aboard the operative “Meteosat 9”-MSG satellite exhibit an underestimation of about 6% and overestimation of 2% (Pers. comm. Philip Watts). Therefore, a preprocessing step takes care of the corresponding recalibration of reflectance values.

The retrieval is only performed for pixels classified as cirrus. By default a cirrus

cloud mask is generated by the Meteosat Second Generation Cirrus Detection Algorithm v2 (MeCiDa) (Krebs et al. 2007; Ewald et al. 2012) that is also directly incorporated in APICS. MeCiDa uses the infrared channels of SEVIRI and is therefore independent of the sun’s position and daylight. The cloud property retrieval however relies on reflected sun light which causes deteriorations at sunrise and sunset. Therefore, results are only used for sun zenith angles smaller than  $80^\circ$ .

### 3.2 Cloud Detection

The work of Ostler (2011) showed that MeCiDa detects virtually all of the cirrus clouds with  $\tau > 0.5$  but only about 50% at  $\tau \approx 0.2$ . For most CSP applications only clouds with a slant path optical thickness  $\tau_s = \tau / \cos(\theta_{\text{sun}})$  smaller than 2.0 are relevant (with  $\theta_{\text{sun}}$  being the sun zenith angle). Otherwise too much light is extinguished. Therefore, clouds with  $\tau < 0.5$  account for a good share of the relevant clouds. It was therefore proposed for this study to improve MeCiDa by increasing the detection efficiency for clouds with  $\tau < 0.5$ . During the period of this study however, the algorithm for “Cloud Optical properties derived from CALIOP and SEVIRI” (COCS) (Kox et al. 2011) was developed and evaluated at DLR. Ostler (2011) compared the detection efficiencies of MeCiDa and COCS. He found that COCS reaches a detection efficiency of 80% at  $\tau = 0.15$  while the detection efficiency of MeCiDa is below 80% for any  $\tau < 0.4$ . It was therefore decided to use COCS as a cloud mask for APICS in a test case and to investigate thereby the impact of an improved detection of thin ice clouds on retrieved circum solar radiation (see Sec. 6.2).

COCS derives two quantities by applying a neural network on the infrared channels of SEVIRI - the ice optical thickness and the cloud top pressure. The effective radius which has strong influence on the circum solar radiation is not retrieved. Therefore, COCS was only used to generate a cloud mask for APICS. All pixels that are assigned an optical thickness larger than 0.1 by COCS are assumed to be cloudy. This cut-off criterion of  $\tau > 0.1$  is necessary to keep the false alarm rate at an acceptable level (pers. comm. Stephan Kox).

### 3.3 Retrieval of Optical and Microphysical Properties

The APICS retrieval uses lookup tables (LUTs) in which simulated reflectivity values for the two SEVIRI channels are stored as perceived by the instrument. The LUT values depend on  $r_{\text{eff}}$  and  $\tau$  but also on other parameters that need to be known beforehand - namely the sun-satellite geometry and ground albedo for two channel wavelengths. The sun-satellite geometry is described by the three angles sun zenith angle  $\theta_{\text{sun}}$ , satellite zenith angle  $\theta_{\text{sat}}$  and the relative azimuth  $\phi$ . During the retrieval, the algorithm moves through the LUT, iteratively searching for the combination of  $r_{\text{eff}}$  and  $\tau$  at which the simulated reflectivity pair matches the observed one best for the given geometry and ground albedo.

The lookup tables cannot cover all atmospheric states that determine the radiative transfer. They are only a coarse approximation covering the most important

parameters. Simplifying assumptions are required because the two independent pieces of information (the two satellite channels) allow only the retrieval of two quantities, in our case optical thickness and effective radius. The LUTs cannot account for effects like multi-layer clouds, inhomogeneous clouds or 3D radiative transfer effects. Clouds are approximated as a homogeneous plane parallel layer always in the same altitude. Also, the clouds are the only atmospheric constituent which is varied within the LUTs - a background aerosol as well as trace gases are kept constant. For example Ostler (2011) showed that consideration of the stratospheric ozone concentration can improve the agreement between APICS retrieval and LIDAR observations. However, since we chose to focus on stand-alone SEVIRI observations and an independent data source would have been necessary to tackle this, an ozone correction was not applied within this study.

The most important sources of uncertainty for thin ice clouds are the incorrect assumption of the ground reflectivity, unknown aerosol properties and the ice particle shape. Because of all these insufficient projections of the reality and uncertainties the results can be erroneous. It even happens frequently that the measured reflectivity pair cannot be reproduced at all by any parameter combination in the LUT. We call these occurrences “outliers”. Contrary, the pixels at which APICS finds a solution are called “insiders”. Outliers can be generated by wrong a priori information - for example about the albedo. This is especially true when the cloud optical thickness is low and underlying features are visible through the clouds.

An example for a failed retrieval can be seen in Fig. 1 where the pair of measured reflectance (black star) is outside the space covered by the LUT. One can also see that the isolines converge for  $\tau \rightarrow 0$  which makes the retrieval prone to small errors.

### 3.4 Improvements Obtained Using a New Albedo Source

In the following it is outlined how the retrieval quality for thin ice clouds was increased during this study by improving the ground albedo information that is fed into the retrieval.

As a measure of the retrieval quality we define the success rate  $S$  as the ratio of the number of insiders to the total number of cloudy pixels in a scene.

$$S = \frac{\text{insiders}}{\text{outliers} + \text{insiders}} \quad (5)$$

A test sector of 207x270 satellite pixels was defined within the whole MSG disk of 3712x3712 pixels to reduce computational and storage burden. Fig. 2 shows a false color composite of the area. The sector includes the southern part of Spain where recently electricity generation by means of CSP flourished. Also the CSP research center Plataforma Solar de Almería, as well as parts of northern Africa, where an increasing amount of CSP projects are planned, are inside the sector. It includes Mediterranean as well as desert climate zones and should therefore

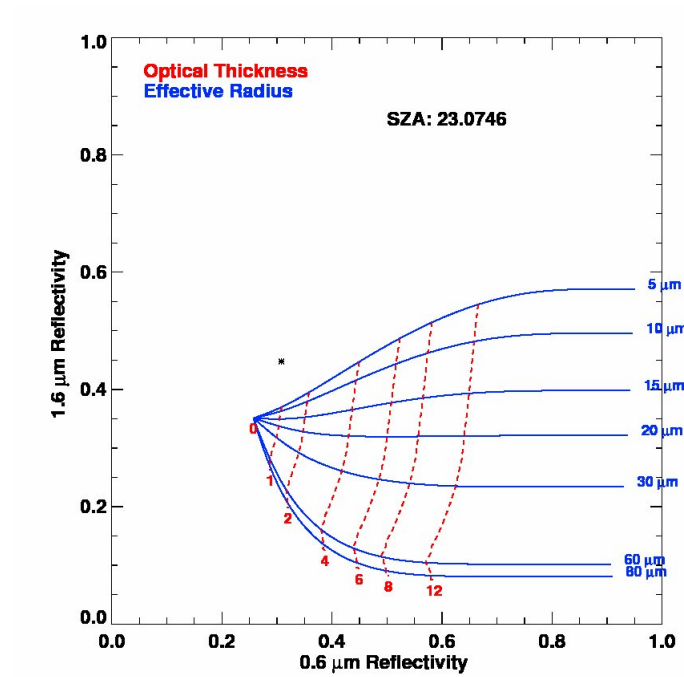


Figure 1: Exemplary slice of an APICS lookup table. Shown are contour lines for  $r_{\text{eff}}$  and  $\tau$  for a certain sun-satellite geometry and albedo. The black star marks the measurement from SEVIRI. In this case the retrieval produces an “outlier” with the measured reflectivity pair far from the area enclosed by the LUT.

offer suitable test conditions. If not noted differently, MSG related statements refer to this area (excluding ocean pixels).

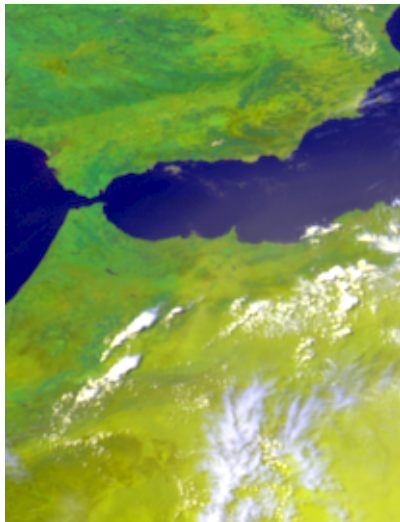


Figure 2: False color composite image of the test sector from SEVIRI channels 1, 2 and 9 at 01 May 2008 14:00 UTC.

For several cases not even 50% of the cloudy pixels could successfully be retrieved within the test sector. As already mentioned the ground reflectivity is crucial if optically thin clouds are considered. Therefore, its treatment within APICS was investigated to possibly improve the low success rate.

To describe the ground reflectivity in detail, the bidirectional reflectance distribution function (BRDF) can be used. It is a function of four angles which define the geometry of incoming and outgoing light. However, the BRDF is not available directly measured at scales of several kilometers. Since the BRDF is often not known and a more simplistic approach is desired for many applications, the ground reflectivity is commonly described by the scalar albedo which is the ratio between upwelling to downwelling radiative flux at the surface. For radiative transfer modelling one assumes in this case that the ground acts as Lambertian reflector distributing all reflected light isotropically, independently from the direction of incidence. APICS relies on the albedo to describe the surface. It must be known a priori for both channels at  $0.6 \mu m$  and  $1.6 \mu m$  at every pixel.

The original version of APICS uses either the “blacksky” or “whitesky” albedo from the MODIS-AMBRALS processing scheme (Strahler et al. 1999). Both are based on clear sky measurements within a 16-day sampling period from the MODIS and MISR instruments which are flown in low earth orbit. From these a BRDF is inversely modelled at a resolution of 1 km. From the BRDF the albedo values are obtained by integrating over the angles of the incoming and outgoing light. For the “blacksky” albedo, diffuse illumination is thereby neglected, and it is assumed that only direct sunlight reaches the ground. The “blacksky”

albedo is therefore dependent on the sun zenith angle. On the other hand, the “whitesky” albedo neglects direct sunlight and assumes isotropic illumination. It is therefore completely independent of the geometry and should be valid in case of optically thick clouds.

The MODIS instrument samples the earth from sun synchronous polar orbits under a different geometry and with a different resolution than SEVIRI. Additionally the ground albedo cannot be directly measured but is a product of inverse modelling which can be a source for further discrepancies. Therefore, the MODIS product may not be suitable for usage with SEVIRI measurements. It was tested if the usage of a ground reflectivity product from MSG measurements would yield better results. For this a product by the University of Bern was considered (Popp et al. 2007). It gives the directional reflectance for the MSG sun-satellite geometry. I.e. a daily course of the ground reflectivity is generated by taking the darkest reflectance value out of a 21-day sampling period for each time of the day. It is assumed that in this case only “background” aerosol with an optical thickness of 0.05 is present. After some filtering and temporal smoothing the ground reflectivity is obtained by decoupling the shares of the atmosphere and the ground to the total top of atmosphere reflectance by the 6S radiative transfer model. This ground reflectivity was used as a priori albedo value for APICS. The ground reflectivity product was processed by University of Bern and available to us covering central Europe (approx.  $40.8^\circ - 51.3^\circ$  N,  $0.3^\circ$  W –  $19.9^\circ$  E,  $430 \times 210$  SEVIRI pixels), therefore the test was conducted in this area and not in the one as shown in Fig. 2. However, the improvements at some points in time were balanced out by deterioration at other times. This is exemplified for the course of one day in Fig. 3.

The atmosphere-ground decoupling can as well be performed using a constrained APICS retrieval. As input to this method, which was developed during this project, serves the SEVIRI “Clear Sky Reflectance Map” product. It is basically the average of the reflectance at the given time over the 10 preceding days under clear sky conditions (*SEVIRI - Clear Sky Reflectance Map Factsheet* 2011). The albedo values in both SEVIRI channels are directly retrieved by “asking” the APICS not for cloud optical properties but for the two albedo values for which the LUT best resembles the two “Clear Sky Reflectance” values in channel 1 & 3 under the condition  $\tau = 0$ . This has the advantage of being consistent to the cloud property retrieval concerning atmospheric composition and radiative transfer modeling. Besides it is assumed that the thus retrieved albedo also corrects for some of the long term variability in the aerosol properties which may deviate from the constant aerosol properties assumed in the simulations for the APICS LUTs. This may also be beneficial for the cloud property retrieval.

The “Clear Sky Reflectance Map” is routinely only available at 12 UTC. Therefore the albedo is only retrieved at this time and used for the whole day. Nevertheless the success rates reached by APICS with this method are superior compared to using any of the other tested albedo datasets. This shows also in Fig. 3 where the retrieval with this APICS-generated albedo product is labeled “EUMETSAT”. This holds true also when longer time spans are compared. For example, considering the whole month of May 2008 for the Mediterranean region as depicted in Fig. 2 the success rates are 71%, 72% and 80% for the MODIS

“blacksky”, MODIS “whitesky” and the “EUMETSAT” albedo.

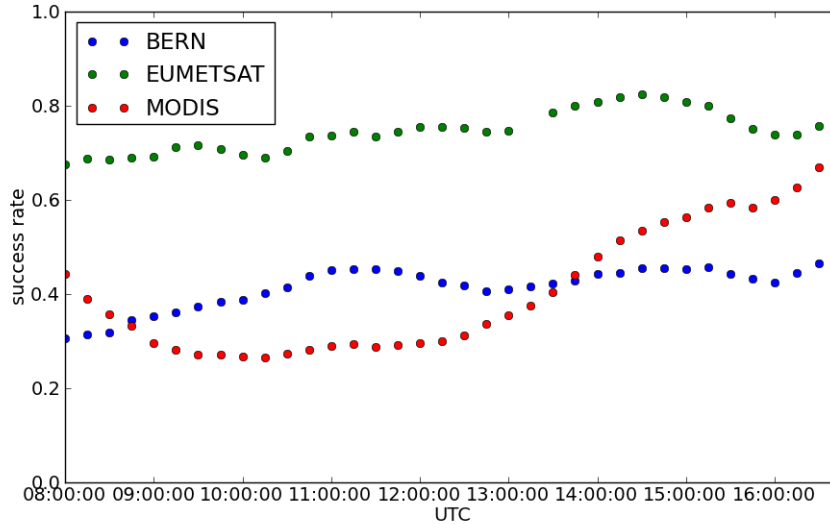


Figure 3: APICS success rates for central Europe under the usage of different albedo datasets for a priori information for 01 May 2008. Red: MODIS albedo as in original APICS version. Blue: Albedo product by the University of Bern. Green: APICS-generated albedo product based on the EUMETSAT clear sky reflectance product.

## 4 Improvements in Radiative Transfer Modelling

The parametrization for the circum solar radiation developed in this study (see Sec. 5) is based on extensive simulations of the aureole under different atmospheric conditions. In this section we briefly describe why we selected the MYSTIC model and which improvements were made in MYSTIC to allow for an exact simulation of the aureole.

For the formation of circum solar radiation it is necessary that the sun light is mainly deflected by small angles. This is equivalent with the scattering phase function  $P$  exhibiting a forward peak. This is the case for particles significantly larger than the light’s wavelength. The larger the size parameter  $\chi = \frac{2\pi r}{\lambda}$  the more light is diffracted by small angles (see for example (Jackson 1999)). Pronounced forward peaks of the phase function pose a problem for most radiative transfer codes when calculating radiances in the vicinity of the sun. For example the widespread Discrete Ordinate solvers (like DISORT from Stamnes et al. (2000)) work with a representation of the phase function as a series expansion of Legendre polynomials. For ice clouds the series expansion must be stopped due to numerical instabilities well before a good representation of the forward peak can be achieved.

Monte Carlo radiative transfer solvers which trace individual photons through the atmosphere treat the phase function explicitly and are therefore preferable for this kind of radiative transfer problem. But even with them the forward peak can cause rare but result-dominating events – so called “spikes“. Leveling the spikes will increase computing time excessively. A solution for this problem was given recently by Buras and Mayer (2011). The variance reduction methods described there are implemented in the radiative transfer model MYSTIC that we used for this study. MYSTIC is part of the libRadtran package (Mayer and Kylling 2005).

To simplify the radiative transfer the sun is commonly assumed to be a point source at infinity. All sun rays are parallel and enter the atmosphere under the same angle. However this approximation is not appropriate when simulating radiance in the vicinity of the sun disk. The sun has a finite angular extent and the center of the sun disk is brighter than the limb. This so called limb darkening is caused by absorption in the sun’s atmosphere and is therefore wavelength dependent. Therefore a disk source was implemented in MYSTIC. The angular radius of this source can be set manually or automatically according to the earth sun distance. By default the wavelength dependent limb darkening model as given in (Scheffler and Elsässer 1990; Koepke et al. 2001) is used but the user can also define an arbitrary radial radiance distribution. If not further noted all simulations refer to an angular sun radius  $\alpha_{\text{sun}}$  of  $0.266^\circ$  and the default spectral limb darkening model.

For simulations with a point source the direct radiation reduces to a  $\delta$ -function. In MYSTIC it is therefore normally calculated by an extra routine applying the Lambert-Beer law to the solar constant. We modified MYSTIC such that the direct radiation is now computed within the same routine as the diffuse radiation. Therefore, the sunshape including direct and diffuse radiance can now easily be simulated in one model call taking into account the extraterrestrial sunshape.

The model improvements can be followed in Fig. 4. The differences between a simulation of the diffuse radiance with a point source (blue) and a disk source (green) are evident especially for angles smaller than  $1^\circ$  from the sun center. The red curve shows the total sunshape consisting of direct and diffuse radiation.

With the such adapted model it was also possible to validate the algorithm of the Sun and Aureole Measurement System (SAM) (Wilbert et al. 2011) for the conversion of the spectral measurements of circum solar radiation to broad band values. The development of SAM was also part of the SFERA WP 13.

## 5 Parametrization of Circum Solar Radiation

In this section a way of efficiently parametrizing the CSR is developed. We thereby resort on the concept of an apparent optical thickness. At first it is discussed why the influence of Rayleigh scattering by air molecules as well as the ground albedo can be neglected in the parametrization. We also evaluate the uncertainty of the parametrization under the fact that the ice particle shape

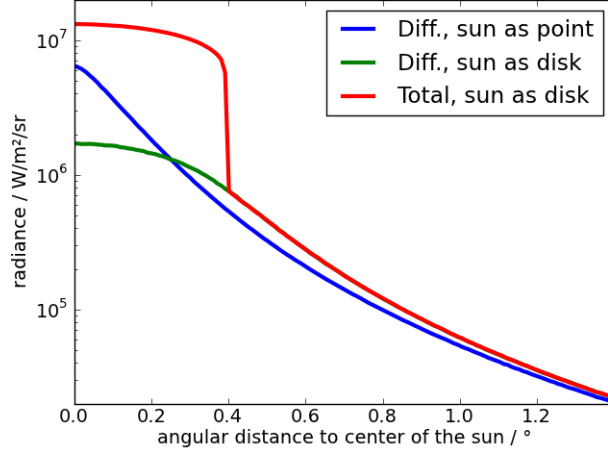


Figure 4: Simulated broadband sunshape for a cirrus cloud with optical thickness 0.5 and with the sun in the zenith. Blue: Diffuse radiance for a point source. Green: Diffuse radiance for a disk source. Red: Direct and diffuse radiance for a disk source.

cannot be retrieved from MSG.

## 5.1 Sensitivity to Neglected Parameters

As mentioned, the circum solar radiation relevant for CSP-applications is mainly caused by scattering within aerosol or thin ice cloud layers. The parameter study shown in the following supports that it is sufficient to focus on the properties of these layers containing large scattering particles.

### 5.1.1 Rayleigh Scattering

To estimate the maximum contribution of Rayleigh scattering by air molecules to the broadband circum solar radiation several simulations were performed with airmass varying between 1 and 50, with airmass being defined as  $1/\cos(\theta_{\text{sun}})$ . The limiting angle  $\alpha$  was set to the maximum of the value range considered in this study – namely  $5^\circ$ . Since high albedo values increase the Rayleigh scattered radiation, the albedo was set to an unrealistic high value of 1. Still, in all simulated cases Rayleigh scattering contributes less than  $1 \text{ W/m}^2$  to the broadband circum solar radiation. It is therefore negligible compared to the uncertainties when retrieving circum solar radiation from MSG. For further simulations  $\theta_{\text{sun}}$  was therefore kept constant at  $0^\circ$  corresponding to an airmass of 1.

### 5.1.2 Albedo

Alike, the influence of the albedo itself was investigated. As mentioned the albedo has some influence on circum solar radiation when considering a Rayleigh atmosphere without any clouds or aerosol. However in absolute terms the dependence of circum solar radiation on the albedo is small. Considering a scattering layer of clouds or aerosol, the forward peak in the phase function is several magnitudes larger than the highest values of  $P$  in the backward hemisphere. Therefore, one may expect that the light that is reflected on the ground and then again scattered back into the field of view (FOV) will not contribute much. This was confirmed by simulations with the maximum FOV of  $5^\circ$ , with varying aerosol and cloud optical thickness. The absolute change in diffuse irradiance stays below  $2 \text{ W/m}^2$  and the absolute change in CSR stays below 0.0025 which for example is below the measurement uncertainty of the SAM instrument (Wilbert et al. 2011). All further simulations in this section have therefore been conducted with the albedo set to 0.

## 5.2 Concept of the Apparent Optical Thickness

Shiobara and Asano (1994) introduced the concept of an apparent optical thickness. We will use this in the following to parametrize the circum solar radiation.

The direct transmission  $T$  through the atmosphere can be decomposed into a particulate and molecular transmission

$$T = T_p T_m \quad (6)$$

The particulate transmission  $T_p$  is expressed as

$$T_p = \exp(-\tau_s) \quad (7)$$

where  $\tau_s$  is the particulate slant path optical thickness along the line of sight from the observer to the sun.  $T_m$  is determined by Rayleigh scattering and absorption on air molecules.

Considering a finite FOV, diffuse radiation will enter any instrument additionally to the direct radiation. Considering the total radiation entering the FOV one may consider an apparent transmission  $T'$  that can as well be decomposed into a particulate and molecular part.

$$T' = T'_p T'_m \quad (8)$$

Since Rayleigh scattering on molecules contributes only a negligible part to the radiation in the circum solar region (comp. Sec. 5.1.1), one can approximate  $T'_m = T_m$ . The molecular transmission  $T_m$  will not be further discussed here since it will cancel out later in the relevant formulas.

The apparent particulate transmission  $T'_p$  can be parametrized as

$$T'_p = \exp(-k\tau_s) \quad (9)$$

with  $k$  taking values between 0 and 1. This means that the difference between the direct particulate transmission – following Beer’s law – and the apparent particulate transmission can be accounted for with the factor  $k$ .

Defining the apparent optical thickness  $\tau_a = k\tau_s$  one obtains

$$T'_p = \exp(-\tau_a). \quad (10)$$

It is notable that the corrective factor  $k$  depends mainly on  $r_{\text{eff}}$ , FOV and particle type and shape but is almost independent of  $\tau_s$  itself. This holds true as long as the optical thickness does not get too large. For this study extensive Monte Carlo simulations with different ice particle types as well as with different aerosol species showed that as long as  $\tau_s < 3$ ,  $k$  varies by less than 3% if all other parameters except the optical thickness are kept constant.

We use this invariance of  $\tau_a$  to calculate CSR efficiently. If we denote the circum solar irradiance for a given FOV with limiting angle  $\alpha$  as  $I_{\text{cir}}$ , the total irradiance from within the same FOV as  $I_\alpha$  and the total irradiance coming from within the sun disk as  $I_{\text{sun}}$ , then we can write

$$\text{CSR} = \frac{I_{\text{cir}}}{I_{\text{sun}} + I_{\text{cir}}} = \frac{I_{\text{sun}} + I_{\text{cir}} - I_{\text{sun}}}{I_{\text{sun}} + I_{\text{cir}}} = 1 - \frac{I_{\text{sun}}}{I_{\text{cir}} + I_{\text{sun}}} = 1 - \frac{I_{\text{sun}}}{I_\alpha}. \quad (11)$$

In general we can express the total irradiance  $I_*$  for a given atmosphere by

$$I_* = I_0 T'_p = I_0 \exp(-\tau_a) = I_0 \exp(-k_* \tau_s) \quad (12)$$

where  $I_*$  can be  $I_{\text{sun}}$  or  $I_\alpha$ . With  $I_0$  we denote the solar constant  $I_s$  corrected for molecular transmission:

$$I_0 = I_s T_m. \quad (13)$$

Applying Eq. (12) to Eq. (11) yields

$$\text{CSR} = 1 - \frac{\exp(-k_{\text{sun}} \tau_s)}{\exp(-k_\alpha \tau_s)} = 1 - \exp[-(k_{\text{sun}} - k_\alpha) \tau_s] \quad (14)$$

with  $k_{\text{sun}}$  being the corrective factor for a FOV correspondent to the sun’s angular radius and  $k_\alpha$  for a FOV correspondent to the limiting angle for which the CSR shall be calculated. Since the angular radius of the sun is assumed constant, we can re-write this as

$$\text{CSR} = 1 - \exp(-\Delta k_\alpha \tau_s). \quad (15)$$

With  $\Delta k_\alpha = k_{\text{sun}} - k_\alpha$  one can even simplify further:  $\text{CSR} \approx \Delta k_\alpha \tau_s$  as long as  $\Delta k_\alpha \tau_s \ll 1$ . This is often the case for aerosol for which, in contrast to cirrus clouds, both  $\Delta k_\alpha$  as well as  $\tau_s$  are often small. Fig. 5 shows an example how well the approximation works for a case with a cirrus cloud and an aerosol layer.

The corrective factor  $k$  is a function of three parameters: The FOV which is characterized by the opening half angle  $\alpha$ , also called limiting angle, the particle shape and the particle size  $r_{\text{eff}}$ .

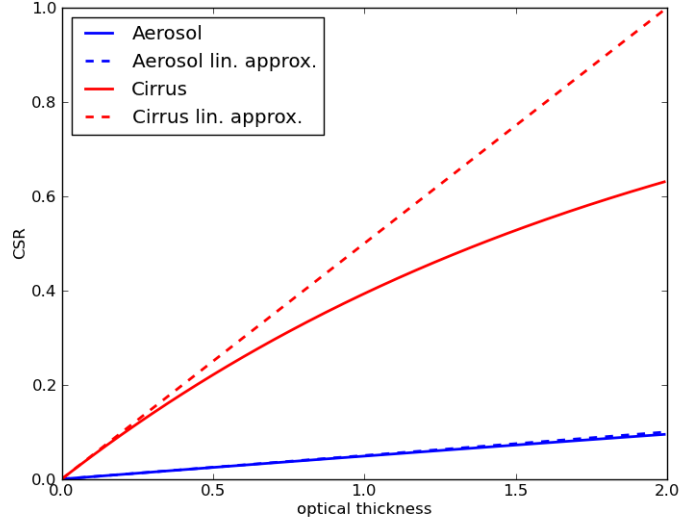


Figure 5: Example for CSR values computed by the exponential ansatz as in Eq. (15) (solid) compared to the linear approximation (dashed) for a cirrus cloud (red) and for an aerosol layer (blue).

A comprehensive lookup table of  $k$ -values has been created that allows the fast computation of  $\text{CSR}(\alpha)$  from the retrieved cloud parameters  $\tau$  and  $r_{\text{eff}}$ . For this one simply has to lookup the  $\Delta k$ -value for the desired parameter combination of  $\alpha$ ,  $r_{\text{eff}}$  and particle shape and apply Eq. (15).

In this document we focus on CSR but it should be noted that the lookup table can serve in the derivation of other circum solar radiation parameters as well. The diffuse irradiance in the circum solar region  $I_{\text{cir}} = I_{\alpha} - I_{\text{sun}}$  for example can be a relevant parameter when considering solar resource overestimation by pyrheliometers. Furthermore, by numerical differentiation of  $I_{\alpha}$  with respect to the solid angle  $\Omega$  enclosed by the FOV one obtains the mean value of sunshape  $\bar{L}$  between the limiting angles  $\alpha_1$  and  $\alpha_2$  as

$$\bar{L}(\alpha_1 < \alpha < \alpha_2) = \frac{I_{\alpha_2} - I_{\alpha_1}}{\Omega_2 - \Omega_1}. \quad (16)$$

The solid angle  $\Omega$  for a given  $\alpha$  computes as  $2\pi[1 - \cos(\alpha)]$ .

### 5.3 Uncertainty due to Unknown Ice Particle Shape

As mentioned above, the ice particle shape has some influence on the circum solar radiation. Fig. 6 shows the dependency of the values that the diffuse circum solar irradiance in  $\text{W/m}^2$  or the CSR can take on the limiting angle  $\alpha_{\text{cir}}$  for the whole range of particle shapes considered (see Sec. 2.3): The figures on the left are for  $\tau_s = 0.4$ , the right ones for  $\tau_s = 2.0$ . Different symbols label a

selection of effective radii. It becomes evident that if only optical thickness is known, the determined CSR has a large uncertainty – it can take any value in the band that is composed of all the symbols. If the effective radius is known, the range of possible values narrows to the band filled by a single symbol. The remaining uncertainty originates from the optical properties of the ice particle shapes. This is the uncertainty that is inherent to the method even for a perfectly working retrieval of the cloud properties  $\tau_s$  and  $r_{\text{eff}}$ . The uncertainties are also depicted in Figs. 7 and 8. The first shows the difference between the maximum and minimum values of the circum solar irradiance depending on the FOV and the optical thickness  $\tau_s$  in  $\text{W}/\text{m}^2$  for varying particle shapes. The latter shows the relative uncertainties in CSR for the same parameters. In both graphs solid lines stand for a fixing of the  $r_{\text{eff}}$  to  $25\mu\text{m}$  and dashed lines for an undefined effective radius. Again, knowledge about the effective radius reduces the uncertainties.

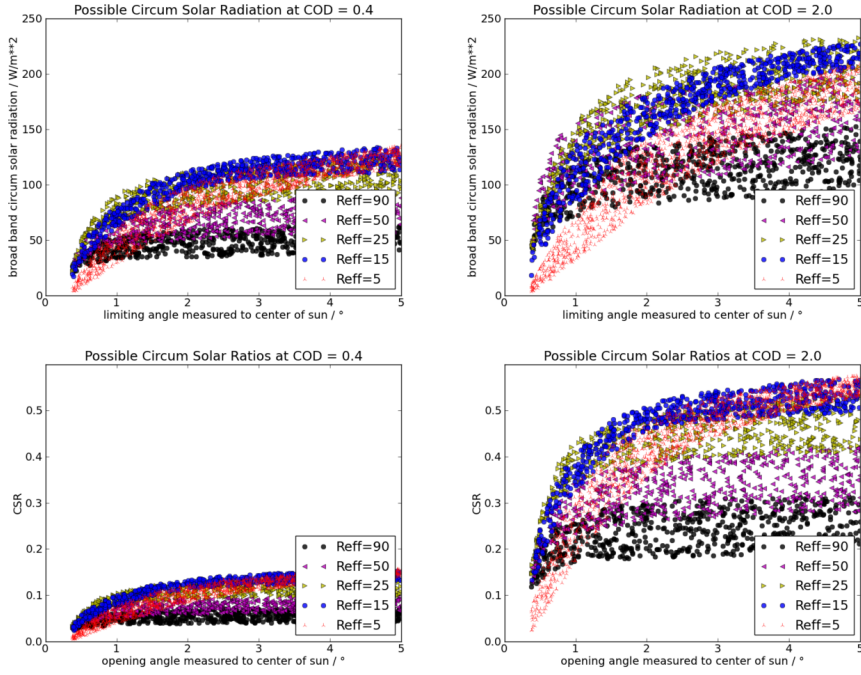


Figure 6: Top: Range of values that the irradiance in the circum solar region can take as a function of the limiting angle  $\alpha$ . Bottom: CSR instead of irradiance is shown. Left:  $\tau_s = 0.4$ . Right:  $\tau_s = 2.0$ . Different symbols denote different effective radii (labeled Reff, units  $\mu\text{m}$ ). Point clouds emerge from the random mixing the five particle shapes and the two particle mixtures as described in Sec. 2.3

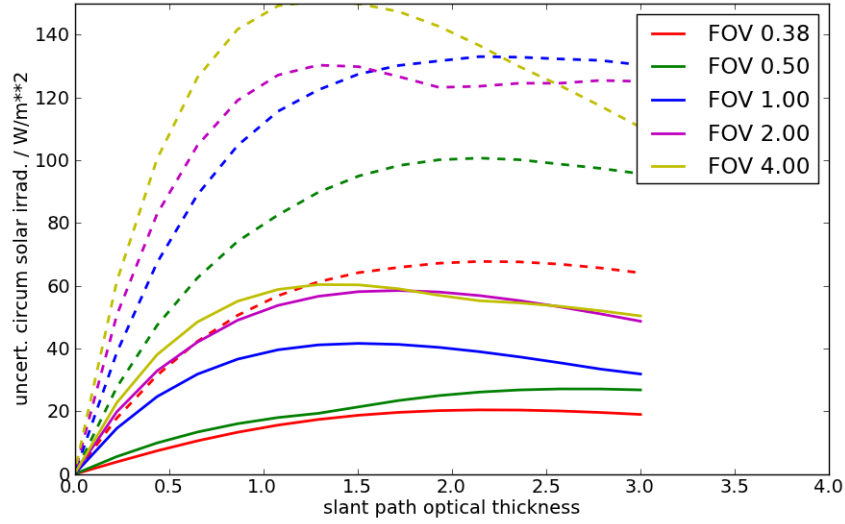


Figure 7: Uncertainty in circum solar radiation for certain FOVs (legend gives opening half angle in degrees). Solid lines: For  $r_{\text{eff}} = 25\mu\text{m}$  and undefined ice particle shape. Dashed lines: For undefined  $r_{\text{eff}}$  and ice particle shape.

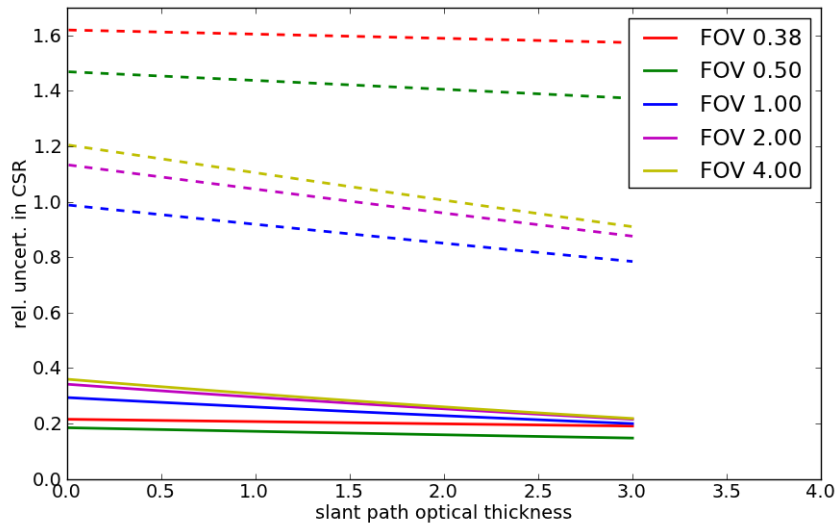


Figure 8: Relative uncertainty in CSR for certain FOVs (legend gives opening half angle in degrees). Solid lines: For  $r_{\text{eff}} = 25\mu\text{m}$  and undefined ice particle shape. Dashed lines: For undefined  $r_{\text{eff}}$  and ice particle shape.

## 6 Circum Solar Radiation Retrieval from MSG

In Secs. 3 and 5 it was outlined that uncertainties exist in the cloud property retrieval as well as in the following conversion of these properties to CSR values due to not knowing the ice particle shape (mixture). It is not obvious how these uncertainties interact. It could be that there is a double penalty if the wrong particles are assumed but the effects could also cancel out partly. By applying the complete retrieval chain yielding circum solar radiation from SEVIRI measurements several times using different setups an overall variability is determined (Sec. 6.1). This way also the influence on CSR when changing from the MeCiDa to the COCS cloud mask is investigated (Sec. 6.2).

Finally in Sec. 6.3 an example is shown where instead of CSR the circum solar irradiance averaged over one year is retrieved from the  $k$ -lookup table.

All calculations of circum solar radiation parameters in Sec. 6 are made for a limiting angle  $\alpha = 2.5^\circ$ .

### 6.1 Circum Solar Ratios for Different Ice Particle Shapes

CSR values have been retrieved from 11 months of SEVIRI data (May 2011 - March 2012) for the test sector described in Sec. 3 for a FOV with  $\alpha = 2.5^\circ$  using the APICS-generated albedo. This was done for all five ice particle shapes and two shape mixtures described in Sec. 2.3. I.e. seven APICS runs were performed for the different particle shapes. In the following conversion to CSR values the same particle shape was assumed as in the correspondent APICS run. A histogram of the relative occurrence of CSR values for the whole domain was computed for every run. Fig. 9 depicts an aggregation of these histograms: In each bin a minimum, maximum and mean value of the seven histograms regarding the individual particle shapes are shown and illustrate the uncertainty induced by not knowing the particle shape. Observing closely, one can also read from the figure that cirrus clouds with  $0.02 \leq \text{CSR} < 0.98$  are detected with an occurrence of approximately 7%. The uncertainty in the CSR histogram is specifically shown in Fig. 10 where the maximum positive and negative deviation from the mean is displayed for each histogram bin. The uncertainty due to the unknown particle shape is smaller than 20% for  $\text{CSR} > 0.15$  in regard to the mean histogram but can be as high as 55% for lower CSR values.

The optical properties of the “Baum” particle mixtures are considered state of the art, so that an operational retrieval would rely on them rather than on individual particle shapes. Therefore, in Fig. 11 similarly the maximum positive and negative deviation relative to the histogram values regarding the two “Baum” mixtures are specifically displayed. Both versions do not agree with each other in the important range of  $0.1 < \text{CSR} < 0.3$  where “baum\_v2.0” is more on the upper bound of all histograms while “baum\_v3.5” is more on the lower bound. It becomes evident that uncertainties up to 60% must be expected due to unknown particle shapes.

Considering the success rate of APICS, the ice particle shape has little influence.

As can be seen in Tab. 1, the success rate varies between 74% and 79% depending on particle shape.

Baum v3.5	74%
Baum v2.0	79%
Solid columns	76%
Hollow columns	76%
Aggregates	75%
Rosettes	78%
Droxtals	74%

Table 1: APICS success rates May 2011 until March 2012 using lookup tables for different ice particle shapes.

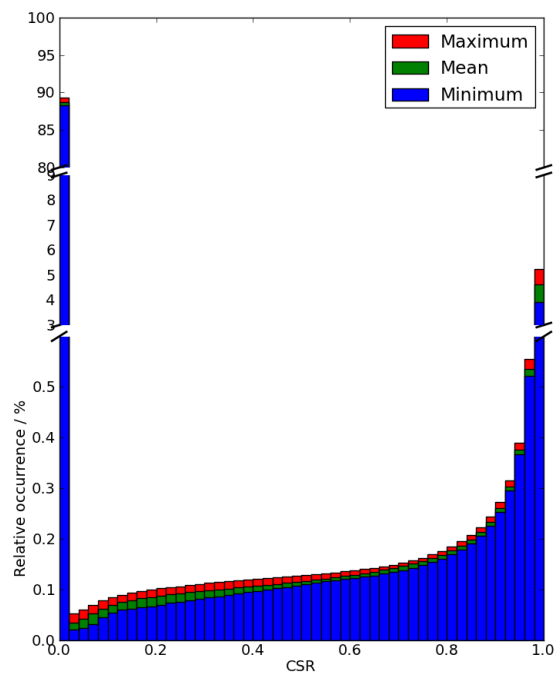


Figure 9: Histogram of the relative occurrence of CSR values retrieved for 11 months for the whole test sector. This was done repeatedly for all ice particle shapes. Shown are the maximum, minimum and mean values in each histogram bin.

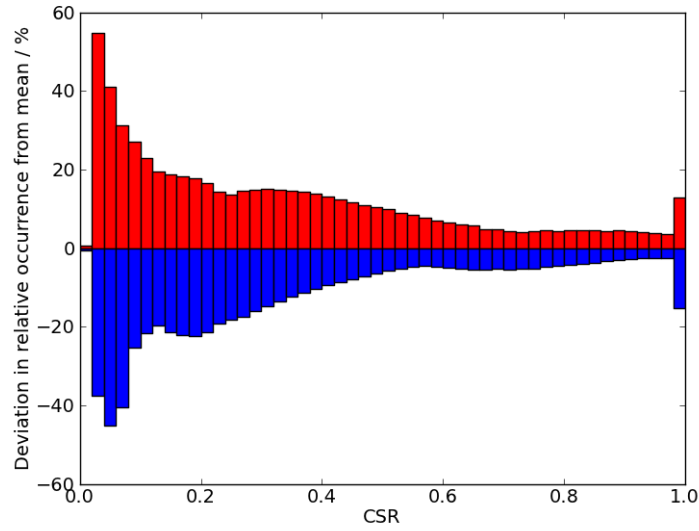


Figure 10: Considering the histogram in Fig. 9, the maximum positive and negative relative deviations in each histogram bin from the mean is displayed.

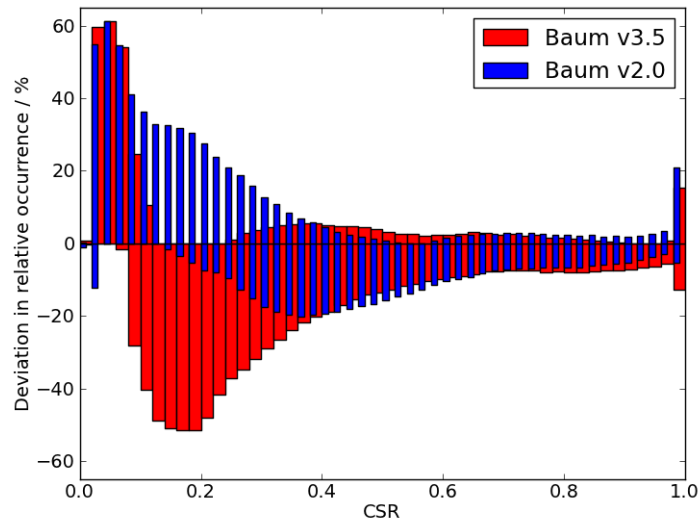


Figure 11: Considering the histograms in Fig. 9, the maximum positive and negative relative deviations in each histogram bin from the values regarding to “baum\_v2.0” (blue) or to “baum\_v3.5” (red) are displayed.

## 6.2 Influence of the Cloud Mask on Retrieved Circum Solar Ratios

As already mentioned, COCS detects more thin cirrus clouds than the cloud detection algorithm MeCiDa that is traditionally used with APICS. Here it is tested how a change to a COCS based cloud mask influences the CSR retrieval results on the basis of one year of data (2009) for the test sector (see Sec. 3). The APICS retrievals for this were conducted with the “baum.v2” optical properties.

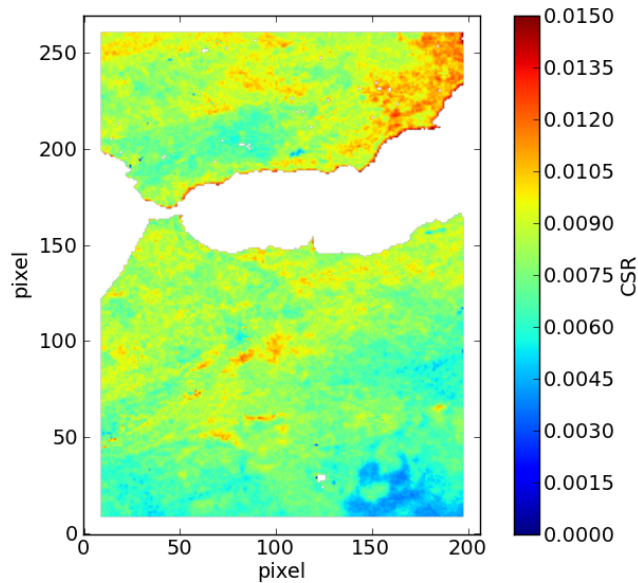


Figure 12: CSR values for cases with the total irradiance being above 200  $\text{W}/\text{m}^2$  averaged over all time steps in 2009 using the COCS cloud mask and the “baum.v2.0” particle mixture.

The number of cloud detections is considerably higher for COCS compared to MeCiDa. During the test period COCS detected 39% more clouds than MeCiDa. APICS reaches the same success rate of 79% for both detection schemes.

Fig. 12 shows CSR values averaged over all time steps in 2009 for which the total irradiance was computed to be above 200  $\text{W}/\text{m}^2$  using the COCS cloud mask. As denominator in the averaging served the number of daylight SEVIRI slots. The limitation was introduced to approximate the non-linear irradiance utilization characteristics of a CSP plant. There are few pixels without values (white pixels inland). These stem from data gaps in the auxiliary clear sky reflectivity product. The enhanced CSR values along the shore line of Spain reflect a land-sea mask feature in the COCS product.

Fig. 13 shows the relative change in the mean CSR averaged over the year 2009 which was obtained by changing from the MeCiDa to the COCS cloud mask.

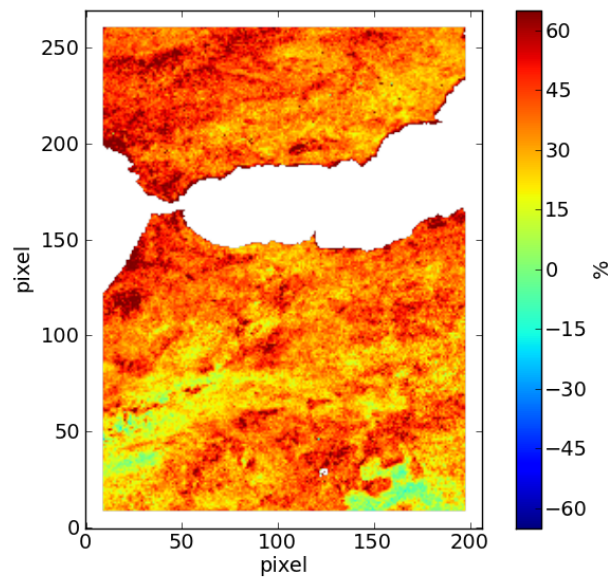


Figure 13: Difference in CSR averaged over all time steps in 2009 considering the “baum.v2.0” particle mixture between COCS and MeCiDa relative to the MeCiDa values. Only CSR values contribute to the average for which the total irradiance was computed as being above  $200 \text{ W/m}^2$ . Positive values indicate that usage of the COCS cloud mask produces higher average CSR values.

The same limitation of the total irradiance being above  $200 \text{ W/m}^2$  was applied. Locally changes can reach up to 65% relative to the MeCiDa values. Averaged over the domain, CSR increases by 35%. This can also be seen in Fig. 14 in which histograms of the relative occurrence of CSR values are shown. For the COCS cloud mask (red) an increase in every bin except for the one on the very left ( $0.0 \leq \text{CSR} < 0.02$ ) can be observed. Fig. 15 breaks down the relative differences between the COCS and the MeCiDa cloud mask depending on CSR. For all bins with  $0.02 \leq \text{CSR} < 0.96$  an increase in occurrence of at least 20% can be registered but especially the occurrence of low CSR values is increased (up to over 100%). This highlights the importance of a reliable detection of thin clouds and that the COCS algorithm is a valuable step into the right direction.

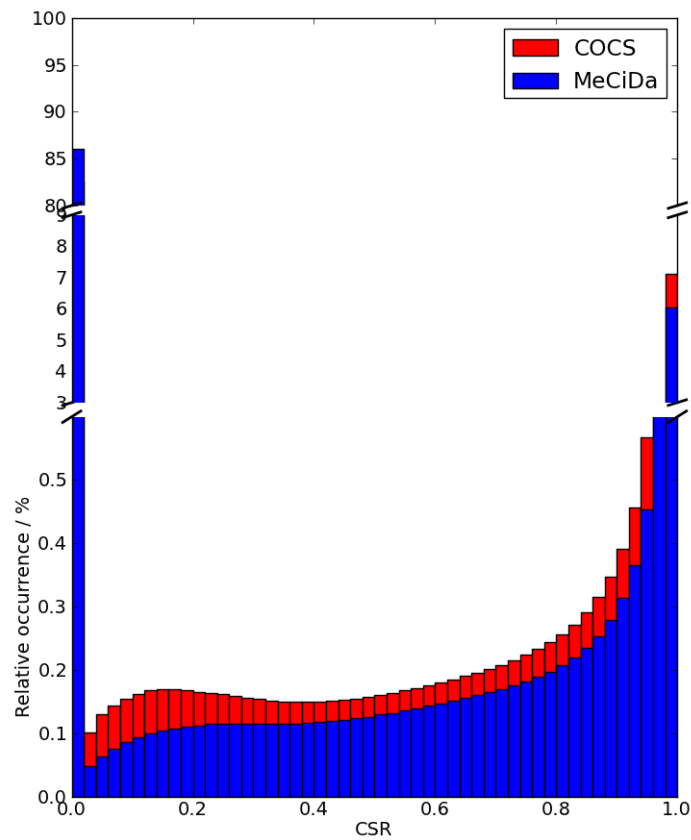


Figure 14: Histogram of the relative occurrence of CSR values retrieved for 2009 with the “baum\_v2” optical properties. Blue: With the MeCiDa cloud mask. Red: With the COCS cloud mask.

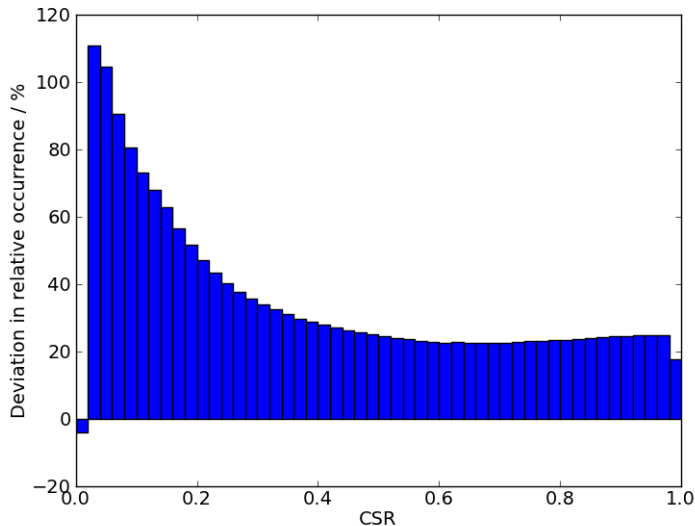


Figure 15: Considering the histogram in Fig. 14, the difference in each histogram bin between the COCS and the MeCiDa cloud mask relative to the MeCiDa values is shown.

### 6.3 Circum Solar Irradiance

As an example for the flexibility of our parametrization we calculated the mean circum solar irradiance in  $\text{W}/\text{m}^2$  within the test sector for a FOV of  $\alpha = 2.5^\circ$ . This was again done for the year 2009, considering values for which the total irradiance was computed as above  $200 \text{ W}/\text{m}^2$ . For the calculations the total irradiance for the clean atmosphere was parametrized from libRadtran calculations depending on  $\theta_{\text{sun}}$  assuming an elevation of 0 m above sea level everywhere. Fig. 16 shows a map of the circum solar irradiance averaged over all time steps using the COCS cloud mask and the “baum\_v2” optical properties. A comparison with Fig. 12 reveals a non-linear relationship between the two considered measures. This emphasizes the importance of selecting circum solar measures carefully according to the desired use.

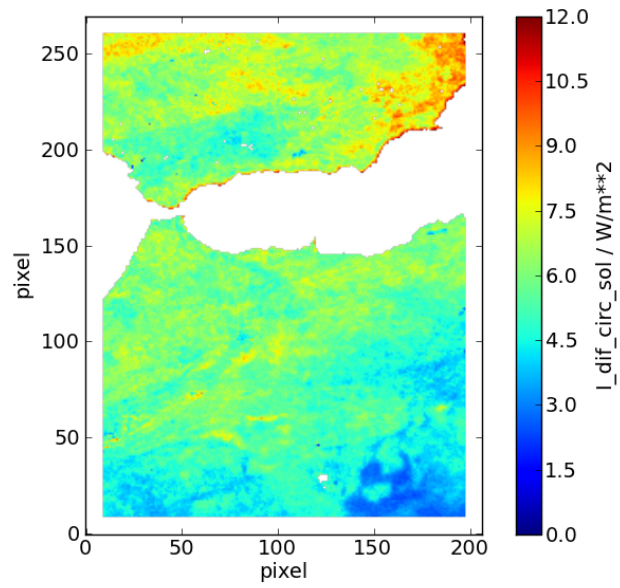


Figure 16: Circum solar irradiance in case of  $I_{\text{sun}} + I_{\text{cir}} > 200\text{W/m}^2$  for a limiting angle of  $2.5^\circ$  averaged over all daylight time steps in 2009 (“baum.v2”, COCS cloud mask).

## 7 Conclusion

In this study a method was developed to determine circum solar radiation from measurements of the geostationary satellite Meteosat Second Generation. To achieve this several components were linked together and extended where necessary. The radiative transfer model MYSTIC was extended such that it can simulate the aureole region in detail. Thereafter, a database for CSR values depending on cloud properties and field of view was established utilizing MYSTIC simulations. This was facilitated by the development of a theoretical basis that allows to parametrize CSR independent of the optical thickness. If a cloud property retrieval is used in conjunction with this database, one finally obtains CSR values from satellite measurements. This was shown with the APICS framework for cloud property retrieval. APICS was also improved during this study by a) showing that more of the relevant thin cirrus clouds can be taken into account if a cloud mask based on the COCS algorithm is used and b) by creating an albedo dataset that is consistent with the cloud property retrieval algorithm and that optimizes the retrieval's success rate. APICS was also extended with new lookup tables for individual ice particle shapes and the "baum v3.5" ice particle mixture to allow for an uncertainty analysis.

Exemplary retrievals of CSR show that the necessary assumption of an ice particle shape or shape mixture induces large uncertainties under particular circumstances. It was also shown that the effective radius is an important parameter and its nescience causes larger uncertainties than not knowing the particle shape. Simplifying assumptions are required because the two independent pieces of information (the two satellite channels) allow only the retrieval of two quantities, in our case optical thickness and effective radius.

Finally, first exemplary maps of the CSR and the circum solar irradiance for a region covering parts of the Iberian peninsular and North Africa were produced to show the capabilities of the method developed here.

## Acknowledgements

Emanuele Emili kindly provided the Uni Bern reflectance data and Stefan Kox the COCS cloud product.

## References

- Baum, B. A. et al. (2011). “Improvements in Shortwave Bulk Scattering and Absorption Models for the Remote Sensing of Ice Clouds”. In: *Journal of Applied Meteorology and Climatology* 50, pp. 1037–1056. DOI: 10.1175/2010JAMC2608.1.
- Baum, B.A. et al. (2005a). “Bulk scattering models for the remote sensing of ice clouds. Part 1: Microphysical data and models”. In: *Journal Of Applied Meteorology* 44, pp. 1885–1895.
- Baum, B.A. et al. (2005b). “Bulk scattering models for the remote sensing of ice clouds. Part 2: Narrowband Models”. In: *Journal Of Applied Meteorology* 44, pp. 1896–1911.
- Bugliaro, L. et al. (2011). “Validation of Cloud Property Retrievals with Simulated Satellite Radiances: A Case Study for SEVIRI”. In: *Atmos. Chem. Phys.* 11.12, pp. 5603–5624. DOI: 10.5194/acp-11-5603-2011.
- Bugliaro, Luca et al. (2012). “Ice Cloud Properties from Space”. In: *Atmospheric Physics*. Ed. by Ulrich Schumann. Springer, pp. 417–432.
- Buie, D. et al. (2003). “Sunshape Distributions for Terrestrial Solar Simulations”. In: *Solar Energy* 74, pp. 113–122. DOI: 10.1016/S0038-092X(03)00125-7.
- Buras, R. and B. Mayer (2011). “Efficient unbiased variance reduction techniques for Monte Carlo simulations of radiative transfer in cloudy atmospheres: the solution”. In: *Journal of Quantitative Spectroscopy and Radiative Transfer* 112, pp. 434–447. DOI: 10.1016/j.jqsrt.2010.10.005.
- Ewald, F. et al. (2012). “An improved cirrus detection algorithm MeCiDA2 for SEVIRI and its validation with MODIS”. In: *Atmospheric Measurement Techniques Discussions* 5. In press.
- Jackson, John David (1999). *Classical Electrodynamics, 3rd Edition*. Wiley.
- Koepke, Peter et al. (2001). “Spectral variation of the solar radiation during an eclipse”. In: *Meteorologische Zeitschrift* 10, pp. 179–186. DOI: 10.1127/0941-2948/2001/0010-0179.
- Kox, S. et al. (2011). “Optical properties of thin cirrus derived from the infrared channels of SEVIRI”. In: *EUMETSAT Meteorological Satellite Conference, Oslo, Norway*.
- Krebs, W. et al. (2007). “Technical note: a new day- and night-time Meteosat Second Generation Cirrus Detection Algorithm MeCiDA”. In: *Atmos. Chem. Phys.* 7, pp. 6145–6159.
- Mayer, B. and A. Kylling (2005). “Technical Note: The libRadtran software package for radiative transfer calculations: Description and examples of use”. In: *Atmos. Chem. Phys.* 5, pp. 1855–1877. DOI: 10.5194/acp-5-1855-2005.
- Mayer, Bernhard (2009). “Radiative transfer in the cloudy atmosphere”. In: *Eur. Phys. J. Conferences* 1, pp. 75–99. DOI: 10.1140/epjconf/e2009-00912-1.
- Nakajima, Teruyuki and Michael D. King (1990). “Determination of the Optical Thickness and Effective Particle Radius of Clouds from Reflected Solar Radiation Measurements. Part I: Theory”. In: *Journal of the Atmospheric Sciences* 47, pp. 1878–1893.
- Ostler, Andreas (2011). “Validierung von optischen Wolkeneigenschaften aus MSG-Daten”. Masterarbeit. Ludwig-Maximilians-Universität München.

- Popp, C. et al. (2007). “Remote sensing of aerosol optical depth over central Europe from MSG-SEVIRI data and accuracy assessment with ground-based AERONET measurements”. In: *Journal of Geophysical Research* 112, D24S11. DOI: 10.1029/2007JD008423.
- Reinhardt, Bernhard (2013). PhD thesis. In preparation. Meteorological Institute Munich - University of Munich.
- Scheffler, Helmut and Hans Elsässer (1990). *Physik der Sterne und der Sonne, 2. Auflage*. BI-Wiss.-Verl.
- Schumann, U. et al. (Sept. 2010). “Effective Radius of Ice Particles in Cirrus and Contrails”. In: *J. Atmos. Sci.* 68.2, pp. 300–321. ISSN: 0022-4928. DOI: 10.1175/2010JAS3562.1.
- SEVIRI - Clear Sky Reflectance Map Factsheet* (July 2011). v2B. EUM/OPS/DOC/09/5165. EUMETSAT.
- Shiobara, M. and S. Asano (1994). “Estimation of Cirrus Optical Thickness from Sun Photometer Measurements”. In: *Journal of Applied Meteorology* 33.6, pp. 672–681. DOI: 10.1175/1520-0450(1994)033<0672:E0COTF>2.0.CO;2.
- Stamnes, K. et al. (2000). *DISORT, a General-Purpose Fortran Program for Discrete-Ordinate-Method Radiative Transfer in Scattering and Emitting Layered Media: Documentation of Methodology*. Tech. rep. Dept. of Physics and Engineering Physics, Stevens Institute of Technology, Hoboken, NJ 07030.
- Strahler, A.H. et al. (1999). *MODIS BRDF/Albedo product: Algorithm Theoretical Basis Document Version 5.0*. URL: [http://modis.gsfc.nasa.gov/data/atbd/atbd\\_mod09.pdf](http://modis.gsfc.nasa.gov/data/atbd/atbd_mod09.pdf).
- Wilbert, S. et al. (2011). “Measurement Of Solar Radiance Profiles With The Sun And Aureole Measurement System (SAM)”. In: *SolarPaces 2011*.
- Yang, P. et al. (2000). “Parameterization of the scattering and absorption properties of individual ice crystals”. In: *Journal of Geophysical Research* 105.D4, pp. 4699–4718.